Ti and Al-Ti thin films for quasiparticle trapping in superconducting quantum circuits

Author: Pol Requena Maldonado
Facultat de Física, Universitat de Barcelona, Diagonal 645, 08028 Barcelona, Spain.

Advisors: Ariadna Gómez del Pulgar, Pol Forn-Díaz and Marius V. Costache

Abstract: Quasiparticles are unwanted excitations of Cooper pairs that disrupt superconductivity and undermine the performance of superconducting qubits. To mitigate this effect, engineered regions of lower superconducting gap energy that capture broken Cooper pairs, known as quasiparticle traps, can be implemented. In this work, as a first step towards the realization of a quasiparticle trapping experiment on the shunting capacitor plates of a 2D transmon-type qubit, a recipe for the deposition of titanium and aluminium-titanium thin films of different thicknesses has been developed and successfully implemented. The room-temperature conductance characteristics of the films have been assessed, and their dependence on film thickness has been ascertained.
Keywords: Quantum physics, solid state physics, uperconducting circuits, Cooper pairs, quasiparticle trapping, thin film deposition
SDGs: Industry, innovation and infrastructures

I. INTRODUCTION

Quantum computing, and, most prominently, superconducting quantum circuits, is a promising technology that is expected to let us process large amounts of data, simulate intricate systems and solve complex problems that are, as of today, undecipherable by classical computers.

However, as of today, the coherence times of superconducting quantum circuits are below the required threshold to surpass classical computing. One of the most impactful reasons behind that is quasiparticle poisoning due to ionizing radiation impacts on circuits and their substrate, which are detrimental for the phenomenon of superconductivity[1]. Those, nonetheless, can be substantially mitigated by implementing quasiparticle traps [2], which are regions of metal with a lower superconducting gap energy to confine undesired unpaired Cooper pairs.

An interesting and unstudied strategy for quasiparticle trapping would be to coat the upside part of the shunting capacitor plates of a qubit made of aluminium with titanium to confine the quasiparticles generated in that region. The shunting capacitor pads of superconducting qubits are generally big structures, with dimensions ranging from 200 um to 700 um. As a consequence, they are prone to quasiparticle generation. Placing quasiparticle traps on them would protect the Josephson junctions of the qubit from those undesired excitations.

In this project, as a first step towards the realization of that experiment, a preliminary study of thin films is conducted to determine their superconducting properties and assess their suitability for quasiparticle trapping applications.

The document is organised as it follows. In Sec. II I introduce the needed theoretical background and describe the quasiparticle concept to continue explaining its fabrication process and the measurements in Sec. III. And the results are shown and discussed in Sec. IV and analysed. In Sec. V the conclusions of this work are summarized.

II. THEORETICAL BACKGROUND

The minimum unit of quantum information are qubits, and they represent the fundamental building block of quantum computers.

Out of all the platforms that have been proposed for the development of a quantum processor, superconducting qubits [3] stand as the most promising and advanced of all. The reasons behind that are the easiness of their fabrication and control, employing standard nanofabrication and microwave engineering techniques, respectively, and the encouraging scalability and gate fidelities that superconducting quantum circuits have already output [4].

Superconducting qubits are anharmonic LC resonators that present no resistance to electric current. These quantum circuits are constituted by simple circuit elements, such as inductors and capacitances, alongside Josephson junctions. The latter are constituted by two layers of superconducting material separated by a thin dielectric layer, through which electrons can tunnel collectively [5, 6] . This tunnelling yields a non-linear inductance that generates an anharmonic potential, hence granting the ability to insulate two single energy levels and originating quantum states of the form [3]

$$\Psi = \alpha|0\rangle + \beta|1\rangle, \tag{1}$$

where α and β are complex coefficients whose squared magnitudes represent the probability of finding the qubit in either state.

As their name indicates, superconductors are constituent of superconducting qubits. These are metals that, below a characteristic temperature known as critical temperature, T_c, have the ability to conduct elec-

tricity losslessly. This is due to the fact that, in superconductors, electrons exists in a bound state known as Cooper pairs, each of them formed by two electrons, as described by BCS theory [7]. In this state, electrons behave as bosons and condense into a single, collective quantum state. Cooper pairs are protected from thermal excitations by a superconducting gap energy, Δ, which is related to the critical temperature of the material as [7]

$$2\Delta(0) = 3.528 k_B T_c \quad \text{for} \quad T << T_c, \tag{2}$$

where k_B is the Boltzmann constant.

Nevertheless, if Cooper pairs are excited by an external source of energy greater than 2 Δ, they can be excited from their ground state, breaking superconductivity and originating a superposition between a hole and an electron known as quasiparticle [3, 8]. The factors that can originate quasiparticles include, but are not limited to, electromagnetic radiation, mechanical vibrations, imperfections in the fabrication process and, most prominently, ionizing radiation from ambience radioactivity and cosmic rays [8].

The presence of quasiparticles and, above all, their tunnelling through the Josephson junction degrades the coherence of the qubit, limits the time during which it can reliably store quantum information and produce resonant frequency shifts [1, 8].

A. Quasiparticle traps

Quasiparticle traps constitute a technological strategy aimed at isolating quasiparticles from the superconducting circuit and minimizing their detrimental effects.

The operating principle of these traps relies on the difference in Δ between the material forming the trap and the material constituting the superconducting circuit. If the trap material has a lower superconducting gap than the circuit material, quasiparticles tend to diffuse into the trap. Once inside, they undergo a relaxation process to lower energy states through phonon emission, which effectively prevents them from escaping the trap and potentially reaching charge-sensitive areas of the superconducting qubit.

Since superconducting qubit circuits are typically fabricated from aluminium, titanium was selected as the trapping material for this project, as it possesses a lower superconducting gap than aluminium.

III. METHODOLOGY

A. Fabrication process

Aluminium is one of the widest materials employed in the fabrication of superconducting quantum circuits, and the material of interest of this thesis. The T_c of this material is $T_c^{Al} = 1.18$ K [9]. In order to implement a quasiparticle trap in an aluminium circuit, we must use a superconductor with a lower T_c than that of aluminium that can also be fabricated following the same metal evaporation technique as aluminium. Hence, titanium was chosen, which has a critical temperature of $T_c^{Ti} = 0.4$ K [9] and electron beam evaporation is also suitable for its deposition.

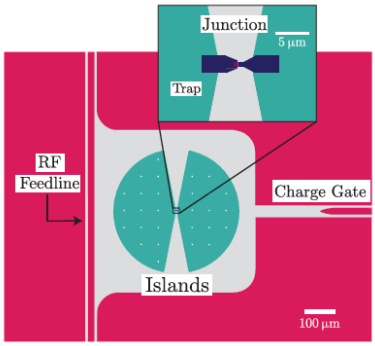

FIG. 1: The trap is the region of overlap between the island and the junction material. The length of the overlap is designed to be the same as the width, such that the area of the trap can be parameterized with a single length parameter. Image from l_{trap} [2]

The fabrication process of the thin film samples is conformed by various steps being done in a cleanroom environment. Hereafter, I am going to explain these steps in more detail.

The substrate chosen for the evaporation of the thin films is highly resistive intrinsic silicon ($\rho \sim 10.000\ \Omega \cdot$ cm), with a layer of native SiOx. Silicon is widely employed for superconducting circuit fabrication, and subsequently our substrate of choice. The substrate was cleaned with acetone and IPA, following a standard method. The size of the substrate was $1 \times 1\,\text{cm}^2$.

The deposition of the thin films is done by employing a Plassys MEB550S System electron beam evaporation system. Electron beam evaporation, a tungsten filament is heated by subjecting it to a given current. By thermionic effect, electrons are emitted from the filament. A high-voltage source of 10 kV is used to conduct the electrons in the form of a beam to a metal target (in my case, aluminium or titanium), which is heated and, subsequently, sublimated. The low pressure of the chamber, of around 10^{-7} to 10^{-8} mBar, makes the metal vapour to be deposited in the chamber, being then able to coat our substrate. The deposited thickness is controlled by using a quartz crystal sensor that shifts its resonance frequency by the effect of the mass increase. To achieve the high vacuum needed for metal evaporation, three pumping stages are employed: a rough pump, a turbo pump and a cryo pump, which are left to pump for 3 to 4 hours before the deposition process. Additionally, before each thin film deposition and after the pumping, a preliminary titanium evaporation of 12 nm is done to adhere to the

TABLE I: Titanium and aluminium-titanium thin film evaporation parameters and results.

	1st Ti evaporation				**2nd Ti evaporation**				**Results**		
Sample	**Current** (mA)	**Evap. rate** (nm/s)	t (nm)	**LL / PrCh pressure after process** (mBar)	**Current** (mA)	**Evap. rate** (nm/s)	t (nm)	**LL / PrCh pressure during process** (mBar)	R (Ω)	R_s ($\Omega/\square$)	ρ ($\Omega \cdot nm$)
Ti	106	0.2	12	$3.6 \cdot 10^{-8}/2 \cdot 10^{-8}$	109–115	0.2	100	$4.1 \cdot 10^{-8}/4.3 \cdot 10^{-8}$	1.62 ± 0.01	7.34	734.24
	86.5	0.2	12	$3.3 \cdot 10^{-8}/1.8 \cdot 10^{-8}$	89–92.2	0.2	100	$3.6 \cdot 10^{-8}/3.2 \cdot 10^{-8}$	1.41 ± 0.01	6.39	639.06
	104	0.2	12	$3.6 \cdot 10^{-8}/2 \cdot 10^{-8}$	107–105	0.2	75	$4.4 \cdot 10^{-8}/3.9 \cdot 10^{-8}$	1.94 ± 0.01	8.79	659.46
	100	0.2	12	$4.1 \cdot 10^{-8}/2.4 \cdot 10^{-8}$	103–101	0.2	75	$4.6 \cdot 10^{-8}/4.4 \cdot 10^{-8}$	2.11 ± 0.01	9.56	717.25
	104	0.2	12	$4.0 \cdot 10^{-8}/1.8 \cdot 10^{-8}$	104–106	0.2	50	$4.5 \cdot 10^{-8}/3.4 \cdot 10^{-8}$	3.01 ± 0.01	13.64	682.12
	104	0.2	12	$3.8 \cdot 10^{-8}/2.2 \cdot 10^{-8}$	104–107	0.2	50	$4.4 \cdot 10^{-8}/3.9 \cdot 10^{-8}$	3.15 ± 0.01	14.28	713.85
	107	0.2	12	$3.9 \cdot 10^{-8}/2.0 \cdot 10^{-8}$	107–108	0.2	25	$4.6 \cdot 10^{-8}/3.6 \cdot 10^{-8}$	7.26 ± 0.01	32.90	822.62
	84.2	0.2	12	$3.3 \cdot 10^{-8}/2.0 \cdot 10^{-8}$	83.8–84.2	0.2	25	$4.3 \cdot 10^{-8}/4.4 \cdot 10^{-8}$	6.89 ± 0.01	31.23	780.70
	85.2	0.2	12	$3.4 \cdot 10^{-8}/1.9 \cdot 10^{-8}$	85.2–86	0.2	10	$4.3 \cdot 10^{-8}/3.7 \cdot 10^{-8}$	25.25 ± 0.01	114.44	1144.42
	87.1	0.2	12	$4.0 \cdot 10^{-8}/2.0 \cdot 10^{-8}$	87.7	0.2	10	$5.1 \cdot 10^{-8}/3.7 \cdot 10^{-8}$	25.37 ± 0.01	114.99	1149.86
Al–Ti	83.2–82	0.2	12	$2.5 \cdot 10^{-8}/1.7 \cdot 10^{-8}$	85.4–86.4	0.2	20	$3.6 \cdot 10^{-8}/4.1 \cdot 10^{-8}$	0.35 ± 0.01	1.59	31.73
	85.5–86	0.2	12	$3.8 \cdot 10^{-8}/2.2 \cdot 10^{-8}$	87.7–88	0.2	15	$4.2 \cdot 10^{-8}/4.4 \cdot 10^{-8}$	0.34 ± 0.01	1.54	23.12
	88.9–89.2	0.2	12	$2.6 \cdot 10^{-8}/1.8 \cdot 10^{-8}$	92.6	0.2	10	$3.6 \cdot 10^{-8}/4.1 \cdot 10^{-8}$	0.34 ± 0.01	1.54	15.41
	92.4	0.2	12	$2.2 \cdot 10^{-8}/1.6 \cdot 10^{-8}$	92.7–93.1	0.2	5	$3.1 \cdot 10^{-8}/3.8 \cdot 10^{-8}$	0.35 ± 0.01	1.59	7.93

chamber walls any residual gas molecules that could be left in the Plassys chambers. This effectively reduces the base pressure by a factor of 3 to 4.

After the pumping of the Plassys load lock and process chamber, and the first titanium evaporation, the thin film deposition is performed following the previously explained process. For the titanium samples, only a layer of that material is deposited. On the other hand, for the aluminium-titanium samples, two consecutive metal evaporations are performed: a first one for aluminium and a second one for titanium. A deposition rate of 0.2 nm/s was decided upon to ensure a homogenous metal deposition.

Using this approach, several samples were fabricated in order to characterize the behaviour of titanium thin films, with thicknesses of 10 nm, 25 nm, 50 nm, 75 nm and 100 nm. These thicknesses were chosen to cover a whole range from bulk to thin film superconductor. Two films of each thickness were manufactured to achieve better statistics.

For the aluminium-titanium samples, a thickness of 30 nm was chosen for aluminium, and the titanium thicknesses were chosen to be 5 nm, 10 nm, 15 nm and 20 nm for different samples. The aluminium value was chosen to stay in the region where the material is considered to be a thin film superconductor. The titanium thicknesses were chosen accordingly to be comparably smaller, as then the predominant material of the sample is aluminium, the main constitutor of the circuit that we aim to emulate.

B. Experimental measurement

The characterization of the conductivity properties of the samples was done via the Van der Pauw method, by using the 4-point probe technique [10]. The operational setup consists on four probes, positioned on top of the sample's edges. Two of the probes are used to supply a given current to the sample, and the remaining probes are used to measure the resulting voltage. Hence, an I-V curve is obtained, from which its slope the resistance of the sample, R, is computed. This method has the advantage of eliminating parasitic and contact resistance. Nonetheless, the geometric precision with which the probes are positioned is crucial to ensure the accuracy of the calculations of sheet resistance.

By performing 4-point probe measurements, the R_s of the material under study can be obtained. This magnitude represents the resistivity of a square region of a thin film sample. Hence, this represents a much more convenient characterization of the resistance samples of uniform thickness that can be considered as 2-dimensional. From the Van der Pauw method, assuming a correct and precise geometrical placement of the probes, sheet resistance can be estimated as

$$R_s = \frac{\pi}{\ln(2)} \cdot R. \tag{3}$$

And the Resistivity, ρ, a property of each material independent of geometric factors and calculated by multiplying the sheet resistance by the film thickness [11].

Lastly, ρ, can be computed. While R and R_s are geometry-dependent magnitudes, ρ is purely intrinsic of each material, and hence a better estimator of conducting properties. From sheet resistance, it can be computed as

$$\rho = R_s \cdot t, \tag{4}$$

where t is the thickness of the sample.

The measurements were done at room temperature, and the hardware setup is conformed by an MPI TS150 probe station and a Keithley 2634B sourcemeter. The latter was controlled via the open-source software QCoDeS [12]. No amplification nor attenuation stages were added to the lines.

IV. RESULTS

Fig.2(a) and Fig.3(a) show a dependency on the thickness that can be attributed to the electron scattering increase in thinner films provoking a higher ρ compared to the bulk material, equally in R and R_s [13]. A part, the figures show an orientation dependency, that can be attributed to the hexagonal crystal structure of titanium that causes electrical anisotropy [14]. For these samples, the aluminium-titanium R_s fit is

$$R_s^{Ti} = (201 \pm 51)e^{-(0.074\pm0.012)t} + (8.4 \pm 1.6). \quad (5)$$

Fig.2(b) and Fig.3(b) show no dependency on the thickness, this can be attributed to aluminium being the main responsible for the electric transport. Again, figures show an orientation dependency, this can be attributed, again, to the hexagonal crystal structure of titanium that causes electrical anisotropy, as mentioned before. For these samples, the R_s fit is

$$R_s^{Al-Ti} = (3.3 \pm 1.5) \cdot 10^{-3}t + (1.5134 \pm 0.0015). \quad (6)$$

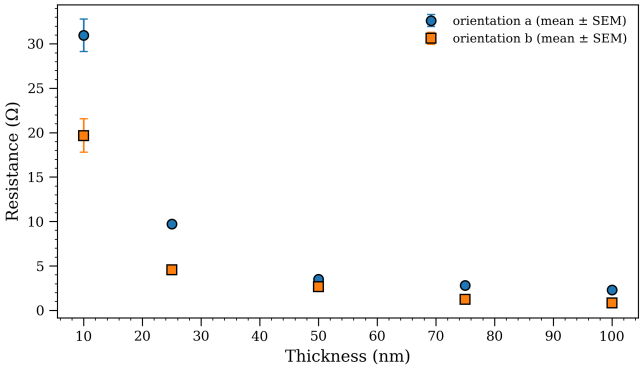

(a)

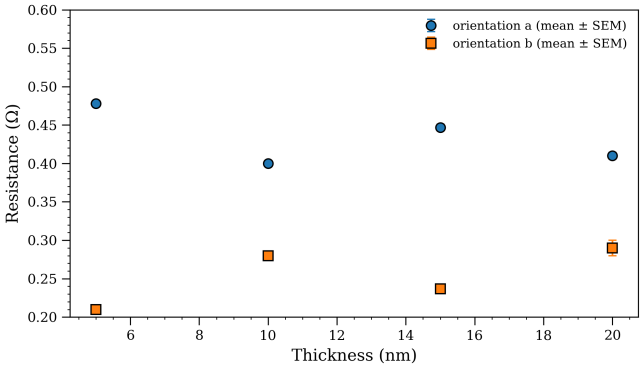

(b)

FIG. 2: (a) Resistance dependency on thickness of the sample for the Titanium samples, with its uncertainty calculated through the different measures of two samples for each thickness with two different orientations, "Orientation B" is rotated by 90° with respect to "orientation A". The uncertainty corresponds to the standard deviation of the mean. The resistance values are listed in Appendix A and Appendix B. (b) Resistance dependency on thickness of the sample for the Aluminium + Titanium samples, with its uncertainty calculated through the different measures of two samples for each thickness with two different orientations, "Orientation B" is rotated by 90° with respect to "orientation A". The uncertainty corresponds to the standard deviation of the mean. The resistance values are listed in Appendix A and Appendix B.

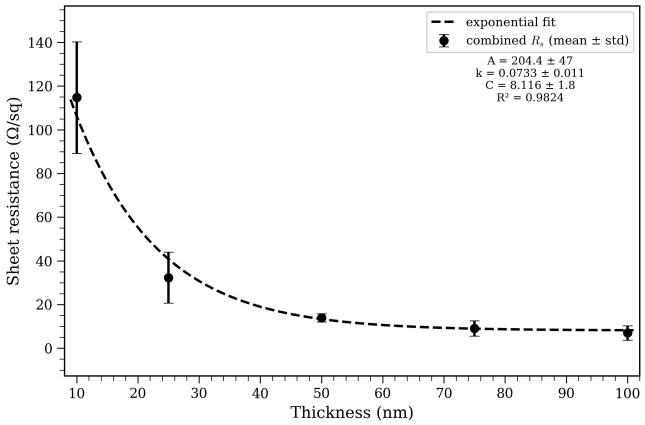

(a)

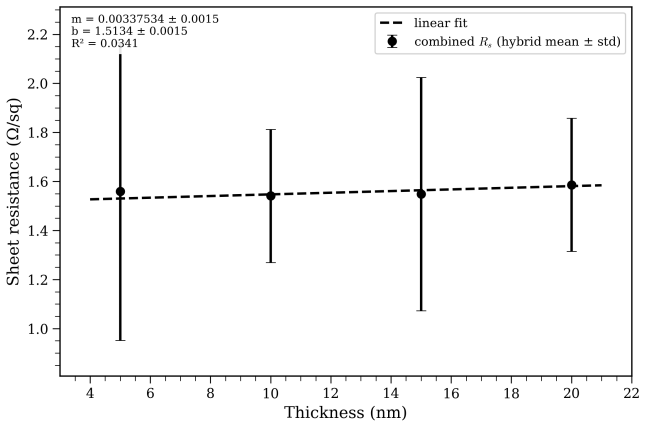

(b)

FIG. 3: (a) Mean sheet resistance dependency on thicknesses of the Titanium sample, alongside its exponential fit. The uncertainty corresponds to the standard deviation of the mean. The resistance values are listed in Appendix A and Appendix B.(b) Mean sheet resistance dependency on thicknesses of the Al-Ti samples, alongside its linear fit. The uncertainty corresponds to the standard deviation of the mean. The resistance values are listed in Appendix A and Appendix B.

Overall, the experimental results show the electrical properties of titanium thin films at room temperature as expected and the dominance of the aluminium in the behaviour of hybrid samples, what means that we can preserve the characteristics of aluminium while introducing a lower superconductive gap material.

V. CONCLUSIONS

In this project, thin films of titanium and aluminium–titanium bilayers were successfully fabricated and characterized with the goal of assessing their suitability for quasiparticle trapping applications in superconducting quantum circuits. The fabrication process, carried out under high-vacuum conditions, enabled the production of films with controlled thicknesses and reproducible electrical properties.

Room-temperature measurements revealed a strong thickness dependence of the resistance and sheet resistance for pure titanium films, consistent with size-effect-dominated transport in thin metallic layers. The observed electrical anisotropy highlights the importance of crystallographic structure in determining the transport properties of titanium thin films.

In contrast, the hybrid samples exhibited transport behaviour dominated by the aluminium layer, indicating that bilayer systems can preserve low resistance while incorporating materials with lower superconducting gaps that can serve as quasiparticle traps.

In addition, acquiring more data from a higher number of newly produced samples could be useful to make a better statistics analysis and prove the reproducibility of the established fabrication recipe. Further studies to be completed would be to check if the purity of the samples can be further enhanced by introducing harder substrate cleaning methods as oxygen plasma or HF dips [3] and/or by performing an argon milling of the aluminium layer before the titanium deposition of hybrid samples. In addition to that, the patterning of test structures via optical lithography would possibly be helpful to obtain a more precise measurement of resistance.

Future work will focus on completing the critical temperature measurements of both pure titanium and aluminium–titanium hybrid samples. This work has already been started with the preparation of the samples for cryogenic measurement, as explained in Appendix C. A systematic study of the resistance as a function of temperature will allow the precise determination of the critical temperature and its dependence on film thickness and bilayer configuration.

These measurements carried out in this thesis, nevertheless, represent the foundational basis of a new quasiparticle trapping approach and are essential to quantitatively assess the superconducting gap hierarchy between aluminium and titanium and to validate the effectiveness of titanium thin films as quasiparticle traps in superconducting circuits.

Acknowledgments

I would like to thank specially Ariadna Gómez del Pulgar for her guidance, patience, and encouragement throughout this project. I am also grateful to Pol Forn-Díaz, and the entire Quantum Computing Group at IFAE for giving me the opportunity to work with them and to Marius V. Costache for making it possible to happen. Finally, I would like to thank my parents and friends for their constant support and encouragement.

[1] G. Catelani *et al.*, *Relaxation and frequency shifts induced by quasiparticles in superconducting qubits*, Physical Review B 84, 064517, 2011.

[2] C. W. Fink *et al.*, *Superconducting quasiparticle-amplifying transmon: A qubit-based sensor for meV-scale phonons and single terahertz photons*, Phys. Rev. Applied **22**, 054009, 2024.

[3] P. Krantz *et al.*, *A Quantum Engineer's Guide to Superconducting Qubits*, Applied Physics Reviews 6, 021318, 2019.

[4] Google Quantum AI and Collaborators, *Quantum error correction below the surface code threshold*, Nature **638**, 920–926, 2025.

[5] M. H. Devoret *et al.*, *Measurements of macroscopic quantum tunneling out of the zero-voltage state of a current-biased Josephson junction*, Phys. Rev. Lett. **55**, 1985.

[6] J. M. Martinis *et al.*, *Energy-level quantization in the zero-voltage state of a current-biased Josephson junction*, Phys. Rev. Lett. **55**, 1543–1546, 1985.

[7] M. Tinkham, *Introduction to Superconductivity*, 2nd ed. Dover Publications, 2004.

[8] A. P. Vepsäläinen *et al.*, *Impact of ionizing radiation on superconducting qubit coherence*, Nature 584, 551–556, 2020.

[9] D. López-Núñez *et al.*, *Superconducting penetration depth of Aluminum thin films*, (2024).

[10] A. Chelly *et al.*, *Broad review of four-point probe correction factors: Enhanced analytical model using advanced numerical and experimental cross-examination*, Results in Physics 48, 106445, 2023.

[11] F. S. Oliveira *et al.*, *Simple analytical method for determining electrical resistivity and sheet resistance using the Van der Pauw procedure*, Scientific Reports 10, 15398, 2020.

[12] https://qcodes.github.io

[13] B. C. Daly *et al.*, *Modulated IR radiometry for determining thermal properties of thin films*, Journal of Vacuum Science & Technology A 32, 041511, 2014.

[14] N. Martin *et al.*, *Anisotropic electrical resistivity during annealing of oriented columnar titanium films*, Surface and Coatings Technology 201, 7720–7726, 2007.

Làmines fines de Ti i Al-Ti per trampes de quasipartícules a circuits quàntics superconductors

Author: Pol Requena Maldonado
Facultat de Física, Universitat de Barcelona, Diagonal 645, 08028 Barcelona, Spain.

Advisors: Ariadna Gómez del Pulgar, Pol Forn-Díaz and Marius V. Costache

Resum: Les quasipartícules són excitacions no desitjades dels parells de Cooper que pertorben la superconductivitat i en perjudiquen el rendiment dels qubits superconductors. Les trampes de quasipartícules són regions dissenyades amb una energia de gap superconductor més baixa que capturen parells de Cooper trencats, mitigant així el seu efecte perjudicial sobre els circuits quàntics superconductors. En aquest treball, com a primer pas cap a la realització d'un experiment de captura de quasipartícules sobre les plaques del condensador shunt d'un qubit de tipus transmon 2D, s'ha desenvolupat i implementat amb èxit un procediment per a la deposició de làmines primes de titani i d'alumini–titani de diferents gruixos. A més, s'han mesurat les característiques de conductància de les làmines a temperatura ambient i les seves dependències.
Paraules clau: Física quàntica, física de l'estat sòlid, circuits superconductors, parells de Cooper,trampes de quasipartícules, deposició de làmines fines
ODSs: Indústria, innovació, infraestructures

Objectius de Desenvolupament Sostenible (ODSs o SDGs)

1. Fi de les desigualtats		10. Reducció de les desigualtats	
2. Fam zero		11. Ciutats i comunitats sostenibles	
3. Salut i benestar		12. Consum i producció responsables	
4. Educació de qualitat		13. Acció climàtica	
5. Igualtat de gènere		14. Vida submarina	
6. Aigua neta i sanejament		15. Vida terrestre	
7. Energia neta i sostenible		16. Pau, justícia i institucions sòlides	
8. Treball digne i creixement econòmic		17. Aliança pels objectius	
9. Indústria, innovació, infraestructures	X		

Appendix A: Values of resistance at room temperature for Ti thin films

TABLE II: Resistance measurements for 10 nm films.

Film	Measurement	Resistance (Ω)
1	1	35.46
	2	35.46
	3	15.03
	4	15.03
2	1	27.96
	2	27.96
	3	27.96
	4	22.77
	5	22.77
	6	22.77

TABLE III: Resistance measurements for 25 nm films.

Film	Measurement	Resistance (Ω)
1	1	4.01
	2	4.83
	3	4.83
	4	10.02
	5	10.02
	6	10.02
2	1	4.54
	2	4.54
	3	9.23
	4	9.23

TABLE IV: Resistance measurements for 50 nm films.

Film	Measurement	Resistance (Ω)
1	1	2.39
	2	2.40
	3	2.40
	4	3.58
	5	3.58
	6	3.58
	7	3.58
2	1	3.02
	2	3.02
	3	3.28
	4	3.28

TABLE V: Resistance measurements for 75 nm films.

Film	Measurement	Resistance (Ω)
1	1	1.16
	2	1.16
	3	1.16
	4	1.16
	5	2.71
	6	2.71
2	1	2.84
	2	2.84
	3	2.84
	4	1.39
	5	1.39

TABLE VI: Resistance measurements for 100 nm films.

Film	Measurement	Resistance (Ω)
1	1	2.58
	2	2.58
	3	0.69
	4	2.54
	5	2.54
	6	2.54
	7	0.68
	8	0.68
2	1	1.81
	2	1.81
	3	1.81
	4	1.02
	5	1.02

Appendix B: Values of resistance at room temperature for Al-Ti thin films

All this samples have a 30nm Al layer as its base and then different thicknesses of Ti deposited above it.

TABLE VII: Measured values from the I-V curves for the aluminium + titanium samples

Film	Measurement	Resistance (Ω)
Al + 5nm Ti	1	0,48
	2	0,48
	3	0,47
	4	0,48
	5	0,48
	6	0,21
	7	0,21
	8	0,21
	9	0,21
Al + 10nm Ti	1	0,4
	2	0,40
	3	0,40
	4	0,40
	5	0,28
	6	0,28
	7	0,28
	8	0,28
Al + 15nm Ti	1	0,46
	2	0,46
	3	0,24
	4	0,24
	5	0,44
	6	0,44
	7	0,44
	8	0,44
	9	0,24
	10	0,24
	11	0,23
	12	0,23
Al + 20nm Ti	1	0,4
	2	0,41
	3	0,42
	4	0,41
	5	0,30
	6	0,28

Appendix C: Critical temperature measurements

For the critical temperature measurements in the cryostat, the samples have been set onto a sample holder, as shown in Fig.4. This sample holder is a PCB, *Printed Circuit Board*, with soldered pins where the sample is placed. To ensure good thermal contact between the sample and the cryostat, a copper wire connects the cryostat to the sample holder.

Apiezon vacuum grease has been applied to the base of the sample holder to guarantee good thermal contact and to ensure that the sample remains firmly attached in any orientation. Wire bonds are performed to provide electrical contact between the sample and the PCB. These connections are made at the edges of the sample, in the same configuration as the probes used for 4-point measurements.

The cryostat that will be used for these measurements is a Leiden Cryogenics CF-CS110. Hybrid samples, for which a critical temperature close to that of pure aluminium is expected, will be placed at the 1 K plate. Phosphor-bronze twisted-pair DC lines will be used to measure these samples. In contrast, titanium samples, whose critical temperature is expected to be similar to that of titanium, are placed in the mixing chamber, reaching temperatures as low as 13 mK. For these samples, copper DC lines will be used.

Appendix D: Images from the Critical Temperature measurements preparation

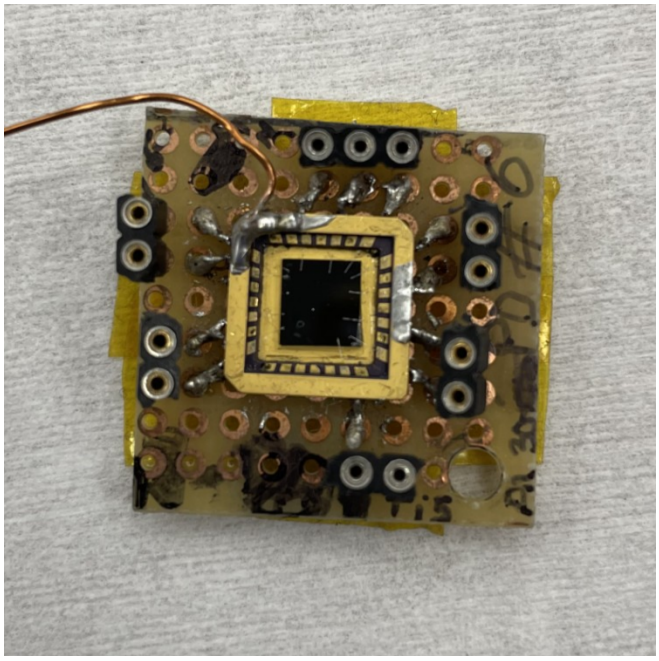

(a)

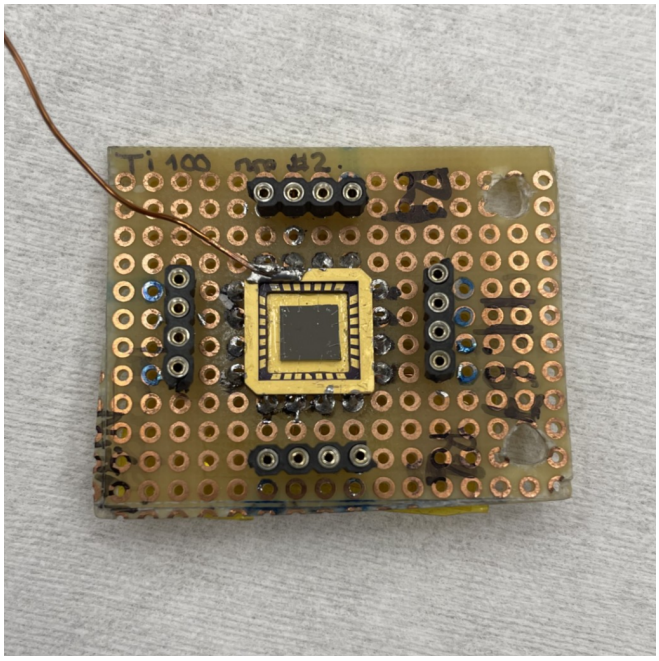

(b)

FIG. 4: Figures (a) and (b) show the sample holder for Critical Temperature measurements